Rare Metal Materials and Engineering

Available online at **www.rmme.ac.cn**

Science Press

Cite this article as: Rare Metal Materials and Engineering

ARTIC

DOI: 10.12442/j.issn.1002-185X.20230739

Effect of Al addition on microstructure, magnetic properties and mechanical properties of $(Fe_{73}Ga_{27})_{99.8}Tb_{0.2}$ alloy

Jinchao Du[1,2], Xiaofei Li[1], Peiying Jiao[1], Zhiguang Zhang[1], Pei Gong[1,*]

1. School of Materials Science and Engineering, Inner Mongolia University of Technology, Hohhot 010051, China

2. Department of Functional Material Research, Central Iron and Steel Research Institute, Beijing 100081, China

Abstract: Several experiments have shown that adding a fractional amount of Al can increase the elongation of the alloys and don't reduce the magnetostrictive strain of Fe-Ga alloys significantly. Furthermore, as the price of Al is lower than that of Ga, using Al to replace part of Ga in the $(Fe_{73}Ga_{27})_{99.8}Tb_{0.2}$ alloy saves production costs as well. The $(Fe_{73}Ga_{27-x}Al_x)_{99.8}Tb_{0.2}$(x=0,1,2,3,4,5) alloys were prepared by vacuum arc furnace to study effect of Al addition on the microstructure, magnetic properties and mechanical properties of. The results show that the phase structure of the alloys is still A2 phase and Tb_2Fe_{17} phase, and the metallographic structure is composed of cellular crystal and columnar dendrite. The decrease of lattice constant, the increase of (100) orientation and the generation of Tb_2Fe_{17} at the grain boundary exert salient effect on the magnetostrictive properties. The fracture morphology of the alloys is intergranular brittle fracture and cleavage fracture, the causes of fracture including the segregation of Tb and Al elements. The parallel magnetostrictive strain ($\lambda_{//}$) of $(Fe_{73}Ga_{24}Al_3)_{99.8}Tb_{0.2}$ alloy reaches 104 $\times10^{-6}$. It is worth noting that compared with $(Fe_{73}Ga_{27})_{99.8}Tb_{0.2}$ alloy, the $\lambda_{//}$and elongation of $(Fe_{73}Ga_{25}Al_1)_{99.8}Tb_{0.2}$ alloy increase by 18.3% and 53.4% particularly, while it also possesses the characteristics of high saturation magnetization (*M*s), low remanent magnetization (*M*r) and coercivity (*H*c), thus cutting the cost in actual production. Therefore, it is important to study the micro-mechanism of Al addition on Fe-Ga alloys for the development of Fe-Ga alloys devices.

Key words: Al doping, $Fe_{73}Ga_{27}$ alloy, magnetic properties, mechanical, properties microstructure

Magnetostrictive materials are one of metal functional materials with high application value and wide application range. By converting electromagnetic energy, sound energy and mechanical energy mutually, devices such as brakes, micro-motors, high-power ultrasonic transducers, sensors, micro-displacement actuators, and hydroacoustic transducers can be manufactured, widely applying in military and civilian fields[1, 2]. The alloy systems most extensively studied are Tb-Dy-Fe alloys whose magnetostrictive strain can reach 1500~2000 $\times10^{-6}$[3, 4], but in view of its brittleness of the material, poor mechanical properties and high prices of Tb and Dy elements, it is limited to laboratory research and military fields. The saturation magnetostrictive strain (λs) of Fe-Ga monocrystalline alloys along the easy magnetization direction can attain 400 $\times10^{-6}$[5, 6], but the high cost, small size and complex preparation process of single-crystal Fe-Ga alloy confine its application scope, whereupon many material scholars have turned their research to polycrystalline Fe-Ga materials[7]. Polycrystalline Fe-Ga alloys have the advantages of high tensile strength and good machinability while it exists the problem of low saturation magnetostrictive strain. Abounding studies have shown that doping other elements in Fe-Ga alloys notably affects the magnetic properties and mechanical properties of the alloys.

Al element, with feature of low price, whose atomic radius approaches to Ga element and they belong to the same main group thus owning similar properties, has drawn extensive attention of researchers. Mungsantisuk[8] argued that the magnetostrictive properties of the alloys didn't prominently lower by adding appropriate Al element. Srisukhumbowornchai N[9]

Foundation item: Inner Mongolia Autonomous Region science and technology plan project (2020GG0284)

Corresponding author: Pei Gong, Ph.D., Professor, School of Materials Science and Engineering, Inner Mongolia University of Technology, Hohhot 010051, P. R. China, Tel:18048342865, E-mail: gongpei123@163.com

found that the magnetostriction strain of $Fe_{80}Ga_{15}Al_5$ alloy could measure up to 234 $\times 10^{-6}$. Zhou Yan[10, 11] prepared $Fe_{82}Ga_9Al_9$ alloy whose saturation magnetostrictive strain crested 88 $\times 10^{-6}$ and the magnetostrictive strain increased to 114 $\times 10^{-6}$ after magnetic field heat treatment. Liu Mingming[12] discovered that the saturation magnetostrictive strain of $Fe_{82}Ga_{13.5}Al_{4.5}$ peaked 247 $\times 10^{-6}$. Moreover, relevant studies have shown that Al can augment the elongation and ductility of Fe-Ga alloys[13]. Liu Yangyang[14] prepared rod-like $Fe_{82}Ga_{18-x}Al_x$ (x=0, 4.5, 6, 9, 12, 13.5) alloys by directional solidification method and results showed that the tensile strength and elongation of the alloys reached 492 MPa and 11.4% respectively when the Al content remained at 4.5 at%, which were higher than $Fe_{82}Ga_{18}$ alloy. Nolting[15] believed that the addition of Cr, Al and V elements can improve the elongation and tensile strength of Fe-Ga alloys, and the fracture mode of the alloys transformed from intergranular fracture to transgranular fracture.

Tb, one of heavy rare earth elements, has high effective magnetic moment, unique 4f electronic structure and strong magnetic crystal anisotropy[16-19]. The truth that 0.2 at%Tb doped in Fe-Ga alloys can markedly ameliorate the properties was proven in precedent researches. Zhang Guangrui[20] acquired $Fe_{81}Ga_{19}Tb_x$ (x=0, 0.2, 0.4, 0.6) alloys thin belt by fast hardening and melt-spinning method. The outcomes demonstrated that Tb elements was enriched at the grain boundaries and the magnetostrictive strain of $Fe_{81}Ga_{19}Tb_{0.2}$ alloy culminated -1320 $\times 10^{-6}$. Meng Chongzheng[21-24] investigated that the tensile strength and elongation of $(Fe_{83}Ga_{17})_{99.8}Tb_{0.2}$ alloy reached 595 MPa and 3.5%, which was significantly higher than that of the undoped alloys. The fracture mode of the alloys changed from intergranular fracture to transgranular fracture and finally to interphase fracture. The dispersed Tb rich phase greatly increased the dislocation density.

In summary, $(Fe_{73}Ga_{27})_{99.8}Tb_{0.2}$ alloy was used as matrix in this article and then added Al element to prepare $(Fe_{73}Ga_{27-x}Al_x)_{99.8}Tb_{0.2}$ (x=0, 1, 2, 3, 4, 5), researching the effect of Al addition on microstructure, magnetic properties and mechanical properties of the alloys.

1 Experiment Materials and Methods

Fe, Ga, Al, and Tb metal elements with a purity greater than 99.95% were selected as raw materials. Ingredients were calculated based on the composition of $(Fe_{73}Ga_{27-x}Al_x)_{99.8}Tb_{0.2}$ and different compositions alloys were weighed through an electronic balance. The total mass of each component alloys was remained 80 g.

Firstly, the weighed samples are placed into a water-cooled copper crucible of a non consumable vacuum arc furnace. Secondly, the mechanical pump and pre extraction valve to pump the air pressure below 5 Pa are opened, and then the forward valve, gate valve, high vacuum molecular pump are sequentially switched to keep the air pressure under 5×10^{-2}. Thirdly, closing the high vacuum molecular pump, gate valve, forward valve and mechanical pump in sequence and flush the furnace with high-purity argon gas three times to reduce alloy oxidation finally. After the melting is completed, flip the ingot and repeat the melting three times to ensure uniform alloys composition and good morphology, for reducing structural defects such as porosity and shrinkage inside the ingot. When the ingot is cooled under a water-cooled copper crucible, it exists undercooling in the longitudinal direction, and the grains grows along this direction. The preferred orientation of the grains saliently exerts an impact on the magnetostrictive performance of the alloys. In consequence, near the middle of the ingot is supposed to take priority in the sample and cut along the longitudinal direction. The cutting location of alloys is shown in Fig. 1.

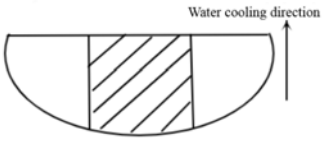

Fig. 1 The sampling position of alloys

2 Results and Discussion

2.1 X-ray Diffraction Analysis

Fig. 2 shows the XRD spectrum of $(Fe_{73}Ga_{27-x}Al_x)_{99.8}Tb_{0.2}$ alloys and the Table 1displays the 2θ angle of (100) peak, lattice constant a(Å) and I_{200}/I_{110} (%) obtained from calculating the XRD spectrum. As shown in the Fig. 2, the characteristic diffraction peaks of the alloys after the addition of Al element are composed of (110), (200) and (211) three diffraction peaks, which indicates that the phase structure of the alloys is dominated by the A2 phase. Since the atomic radius of Tb (0.251 nm) element is much larger than that of Fe (0.126 nm) atomic radius and Ga (0.140 nm) atoms, Tb element difficultly dissolves in Fe-Ga solid solution. Based on the latter EDS analysis results, Tb element is mainly gathered at grain boundaries and generated Tb_2Fe_{17} phase. However, the diffraction peak of Tb_2Fe_{17} phase isn't appeared on the XRD spectrum, which may be credited to the low content of this phase, thereby inability to appear the characteristic peak on the XRD spectrum.

The second row in the table displays the angle of the (110) peak of the alloys shifting to the right, then to the left, finally gradually returning to normal, which is attributed to the lattice distortion caused by mutual substitution of different elements in the alloys, thus resulting in diffraction peaks shifting. From the outcomes in third and fourth rows of the table shown, the a (Å) of the alloys presents a trend of first decreasing and next increasing, then decreasing and ultimately increasing while the I_{200}/I_{110} (%) exhibits converse tendency. The transmutation in lattice constant of the alloys is primarily pertinent to the substitution of Ga atoms in the lattice after the addition of Al

atoms. An augmentation in the lattice constant of the alloys means the decrease of the lattice gap and vacancies in the alloy's crystal. According to literatures[25], vacancies can reduce the electron density in the surrounding area and improve the physical environment around Fe, hence enhancing the magnetostrictive properties of the alloys. The lattice constant of the alloys tends to increase on account of Al atomic radius greater than Ga atomic radius. When x=3 at%, the lattice constant is acquired a minimum value of 2.8888; the I_{200}/I_{110} (%) crests 86.60, manifesting that (100) orientation in the alloys is enhanced at this time, which means that appropriately adding Al element augments the (100) orientation. As the easy magnetization direction of Fe-Ga alloys is (100) direction, it exerts an indispensable impact on the magnetostriction performance, and therefore it is a momentous reason for the large magnetostriction after the addition of Tb element as well.

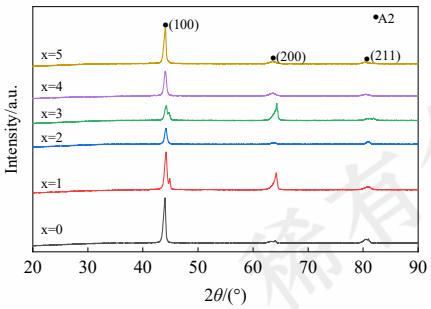

Fig. 2 The XRD pattern of $(Fe_{73}Ga_{27-x}Al_x)_{99.8}Tb_{0.2}$ alloys

Table 1 XRD analysis results of $(Fe_{73}Ga_{27-x}Al_x)_{99.8}Tb_{0.2}$ alloys

x(at%)	0	1	2	3	4	5
$2\theta_{100}$(deg)	44.03	44.2	44.17	44.25	44.08	44.08
a(Å)	2.9055	2.8994	2.9076	2.8888	2.9137	2.9138
I_{200}/I_{110}(%)	3	42.5	10	86.6	8.6	10.6

2.2 Metallographic Structure

Fig. 3 presents the metallographic structure diagram of $(Fe_{73}Ga_{27-x}Al_x)_{99.8}Tb_{0.2}$ alloys magnifying 50 times. It shows that the metallographic structure of the alloys is mainly composed of cellular crystals and columnar dendrites. The reason for the formation of cellular crystals is that during the forced growth process of the crystal, occurring the interface instability conditions, the convex peaks and concave valley shapes is appeared at the interface. The growth rate of the concave valley grows slow attributing to the accumulation of excess solute, thus inhibiting the growth process. The appearance of the concave valley also triggers additional protrusions in adjacent areas, which ultimately forms cellular structure through repeated processes. The development of columnar dendrite is resulted from the enlargement of component supercooling zone and local bulge formed by the disturbance of the interface gets larger extension in the solution. In the process, new component supercooling is occurred, which destroys the stability of the original cellular crystal interface, making the crystal growth direction growing towards the crystallography orientation with the largest growth rate. At the same time, the cross section of the cellular crystal also shows lateral bulge on the grounds of crystallography factors, wherefore the cellular crystal transforms into columnar dendrites.

The grain structure in Fig. 3(a) and (f) presents irregular cellular chiefly while the grain structure in Fig. 3(b) and (c) are mainly composed of irregular cellular crystals and a small amount of columnar dendrites. Fig. 3(d) includes columnar dendrites and the grain structure of Fig. 3(e) is made up of hexagonal cellular crystals. According to the knowledge of liquid metal forming[26], the more developed the dendrites are; the liquid flow is less supplemented during the final shrinkage stage of the solidification process, generating shrinkage porosity and porosity defects, which leads to the descent in the mechanical properties of the alloys. It is consistent with the hardness values measured later. That is, the hardness of $(Fe_{73}Ga_{24}Al_3)_{99.8}Tb_{0.2}$ alloy will decrease.

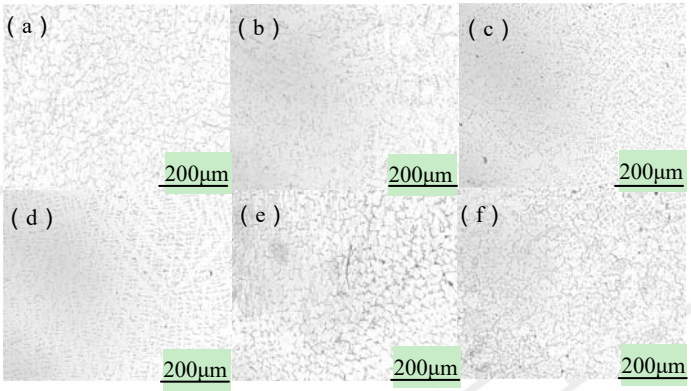

Fig. 3 Metallographic structure of $(Fe_{73}Ga_{27-x}Al_x)_{99.8}Tb_{0.2}$ alloys

2.3 Scanning Electron Microscopy and Energy Spectrum Analysis

Fig. 4 shows the backscattered electron images of $(Fe_{73}Ga_{27-x}Al_x)_{99.8}Tb_{0.2}$ alloys at different magnifications and Table 2 bespeaks the results of point analysis for alloys of different compositions. Observing the backscatter image of the alloys that Tb element enriches at the grain boundary in varying degrees, which resulting from the atom radius of Tb element is much larger than that of Fe atom and Ga atom radius and its solubility in Fe-Ga solid solution remains tiny. In terms

of pertinent literatures[27], when Tb element gathers at grain boundaries, it may be generated diverse compounds with Fe atoms incorporating $TbFe_2$, $TbFe_3$, Tb_2Fe_{17}, Tb_6Fe_{23}, all of which can significantly ameliorate the magnetostriction properties of the alloys.

According to the analysis results of points E and F in the table, comparing the relative content of Fe atoms with the content of Tb elements, their ratios approach to 1:8.67 and 1.8.38 respectively, which are extremely close to the atom ratios of Fe and Ga in Tb_2Fe_{17} compounds. From above mentioned results to know that Tb_2Fe_{17} whose saturation magnetostrictive strain keeps more than 200 ppm precipitates at the grain boundaries of $(Fe_{73}Ga_{24}Al_3)_{99.8}Tb_{0.2}$ alloy, which is also the reason for increasing magnetostriction coefficient of the alloys. In addition, the analysis results at point D shows that the Al element content is relatively high, far above the Al element content in the nominal composition. The enrichment of Al element reinforces the pinning effect of the alloys, making it difficult for the alloy's magnetic domain to rotate, thereby reducing the magnetostriction performance of the alloys, which keeps peace with the lowering in the magnetostriction coefficient of $(Fe_{73}Ga_{25}Al_2)_{99.8}Tb_{0.2}$ alloy measured in latter passage.

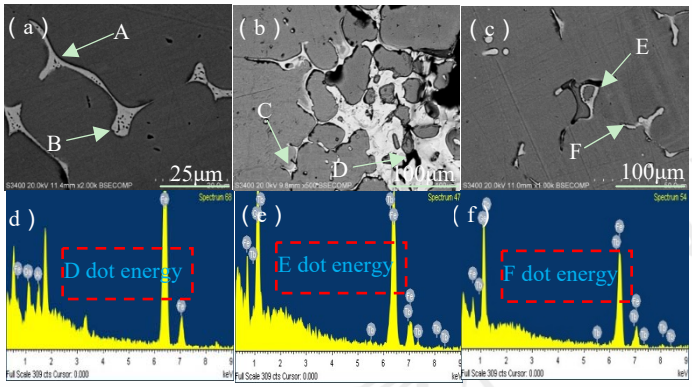

Fig. 4 Scanning electronic image of $Fe_{73}Ga_{27-x}Al_x)_{99.8}Tb_{0.2}$ alloys, ((a)-(c) corresponding to 0,2,3; (d), (e), (f) are the amplification of energy spectrum at points D, E, F, particularly.)

Table 2 EDS analysis results of $(Fe_{73}Ga_{27-x}Al_x)_{99.8}Tb_{0.2}$ alloys

Content (at%)	Fe	Ga	Al	Tb
A	50.38	43.24	0	6.38
B	50.37	43.19	0	6.43
C	54.92	36.53	0	8.56
D	68.93	17.57	13.50	0
E	53.28	40.57	0	6.15
F	53.46	40.16	0	6.38

2.4 Magnetostrictive Properties

错误!未找到引用源。(a) and (b) present the curves of the parallel magnetostriction coefficient ($\lambda_{//}$) of $(Fe_{73}Ga_{27-x}Al_x)_{99.8}Tb_{0.2}$ alloys changing with external magnetic field and Al content respectively. From **错误!未找到引用源。** (a) known, the external magnetic field required for the $\lambda_{//}$ of the alloys to reach saturation after the addition of Tb element is in the range of 1300-1700× 79.6 $A\cdot m^{-1}$and the applied magnetic field required remains larger when the magnetostrictive coefficient of the alloys reaches saturation with the addition of Al element.**错误!未找到引用源。**(b) shows that the $\lambda_{//}$ of $(Fe_{73}Ga_{27-x}Al_x)_{99.8}Tb_{0.2}$ alloys varies between 62-104 $\times10^{-6}$, the $\lambda_{//}$ of the alloy increases slightly at x=1 at%. In light of the XRD analysis above, the decrease of the lattice constant of the alloys and the enhancement of the orientation [100] are conducive to the magnetostrictive properties of the alloys. When x=2 at%, the $\lambda_{//}$ of the alloy shows a decreasing trend due to the portion of Al elements existing in the form of precipitated phase and the precipitated phases produce an pinning effect on the magnetic domains, which reduces the magnetoelastic property of the alloys[27]. The alloy's $\lambda_{//}$ of x=3 at% reaches the maximum value of 104 $\times10^{-6}$ that is related to the minimum lattice constant and the strongest orientation [100]. Tb_2Fe_{17} phase which is beneficial to the improvement of magnetostrictive properties is produced at the grain boundary of the alloy meanwhile. The $\lambda_{//}$ of the alloys decreases significantly when x=4-5 at%; by occasion of the solid solution capacity of Fe and Al elements is more diminutive than that of Al and Ga elements whereupon Al elements destroy Ga-Ga atomic pairs[28]. Clark proposed that the Ga-Ga atomic pair is an important reason for the large magnetostrictive properties of Fe-Ga alloys[29].

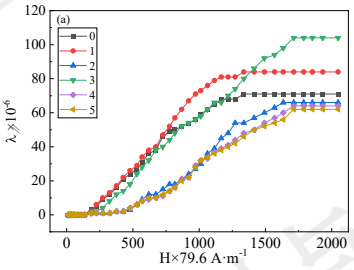

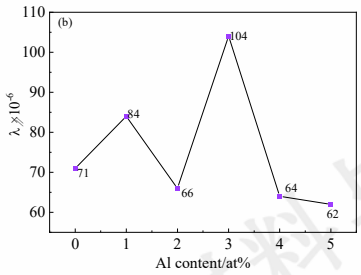

Fig. 5 The curve of parallel magnetostriction coefficient of $(Fe_{73}Ga_{27-x}Al_x)_{99.8}Tb_{0.2}$ alloys changing with applied magnetic field; (b) the curve of parallel magnetostriction coefficient varying with Al content

2.5 Hysteresis Loop Analysis

Fig. 6(a) is hysteresis loop diagram of $(Fe_{73}Ga_{27-x}Al_x)_{99.8}Tb_{0.2}$ alloys. Fig. 6(b) presents the linear fitting results of saturation magnetization (*M*s), remanent magnetization (*M*r) and coercivity (*H*c) of the alloys obtained by Origin software, which vary with Al content. From the Fig. 6(a) known, the magnetization of all samples basically reaches saturation state when the applied magnetic field approaches 10000 G.

Fig. 6(b) shows that the *M*s of $(Fe_{73}Ga_{27-x}Al_x)_{99.8}Tb_{0.2}$ alloys varies within 109.1±21.6 (G). The *M*r and *H*c of $(Fe_{73}Ga_{27-x}Al_x)_{99.8}Tb_{0.2}$ alloys morph slightly. The *M*r changes in the range of 0.3±0.9(G), and the *H*c transmutes in the range of 8.1±2.36 (G). The *M*r and *H*c of $(Fe_{73}Ga_{27-x}Al_x)_{99.8}Tb_{0.2}$ alloys show an overall trend of first decreasing, then increasing, and final decreasing with the change of Al content, while the trend of *M*s is essentially opposite. On the basis of literatures, the materials with high *M*s and low *M*r are able to save resources in the actual production of products, which is conducive to the development of products in the light, thin, short direction and quickly respond to the inversion of the external magnetic field[30]. For soft magnetic materials, the lower *H*c indicates that they are susceptible to magnetization by external magnetic fields and are easily demagnetized by external magnetic fields or other elements, which reduces the hysteresis loss and magnetization power of materials, availing its practical application. According to the above analysis, the $(Fe_{73}Ga_{26}Al_1)_{99.8}Tb_{0.2}$ alloy possesses high *M*s, low *M*r and *H*c in this series of alloys, whereupon it is more suitable for extensive production and application.

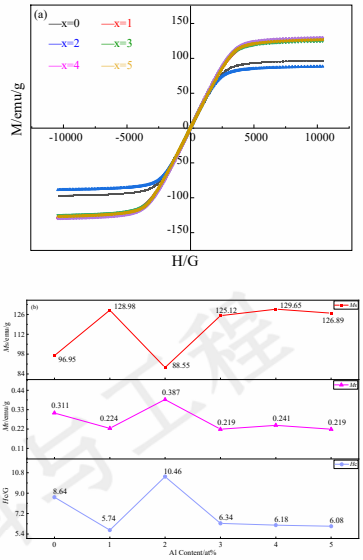

Fig. 6 (a) Hysteresis loop curve of $(Fe_{73}Ga_{27-x}Al_x)_{99.8}Tb_{0.2}$ alloys; (b) The curve of *M*s, *M*r and *H*c of $(Fe_{73}Ga_{27-x}Al_x)_{99.8}Tb_{0.2}$ alloy varying with Al content

2.6 Room Temperature Stretching Experiment

错误!未找到引用源。 is the stress-strain curve of $(Fe_{73}Ga_{27-x}Al_x)_{99.8}Tb_{0.2}$ alloys. Fig. 7(a) and (b) show the curves of the tensile strength and elongation of the alloys varying with Al content separately. As the Fig. 7(a) shows, the highest tensile strength of the alloys reaches 322.8 MPa at x=3 at%. With the augmentation of Al content, the tensile strength of the alloys decreases firstly, then increases, and decreases finally in a wavy trend. The tensile strength of the alloys descends after doping a fraction of Tb element comparing to $Fe_{73}Ga_{27}$ alloy, which attributes to the atomic radius of Tb surpassing that of Fe and Ga atoms and Tb element is enriched at the grain boundary, thus increasing the tendency of grain boundary cracking. Fig. 7(b) shows that the elongation of $(Fe_{73}Ga_{26}Al_1)_{99.8}Tb_{0.2}$ alloy is greater than that of $(Fe_{73}Ga_{27})_{99.8}Tb_{0.2}$ alloy, suggesting that the addition of appropriate Al element has a certain degree of improvement in plasticity.

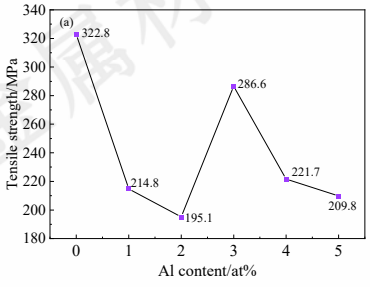

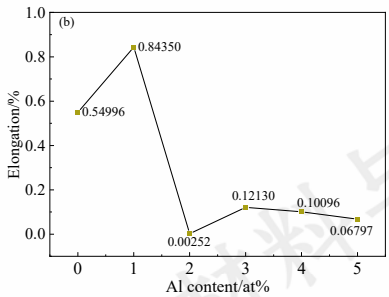

Fig. 7 (a) and (b) are the curves of tensile strength and elongation of $(Fe_{73}Ga_{27-x}Al_x)_{99.8}Tb_{0.2}$ alloys changing with Al content particularly.

2.7 Fracture Morphology Analysis

Utilize the scanning electron microscope and energy spectrum analysis to observe the micro morphology and analyze the cause of fracture of the alloys. Fig. 8 shows the high magnification fracture morphology of $(Fe_{73}Ga_{27-x}Al_x)_{99.8}Tb_{0.2}$ alloys. Points A and B in Fig. 8(a) correspond to white dots in the $(Fe_{73}Ga_{27})_{99.8}Tb_{0.2}$ alloy grain and point C symbolizes the white dots in the grain boundaries, whose Tb element are far higher than those in the matrix displayed by EDS analysis, proving that Tb element is segregated at grain boundaries or within the grain. According to the previous theory, element eliguation increases the tendency to fracture along grain boundaries, wherefore Tb element segregation is the principal reason of fracture in $(Fe_{73}Ga_{27})_{99.8}Tb_{0.2}$ alloy. The point D in Fig. 8(b) is the composition analysis at the grain boundary of the $(Fe_{73}Ga_{26}Al_1)_{99.8}Tb_{0.2}$ alloy whose relative content of Al element keeps more than that in the nominal composition, which also evincing Al element segregation is existed at the grain boundary as a salient cause for the fracture of the alloy. The fracture modality of $(Fe_{73}Ga_{25}Al_2)_{99.8}Tb_{0.2}$ alloy is cleavage fracture and apparent cleavage steps usually comprised of a sequence of diminutive fracture surfaces is observed in Fig. 8(h), which represent at the micro level as a fleet of cleavage surfaces such as those in a body centered cubic lattice of metals, where the cleavage surfaces are mainly (001) crystal planes. In terms of the previous XRD analysis, the crystallography structure of $(Fe_{73}Ga_{25}Al_2)_{99.8}Tb_{0.2}$ alloy resembles α- Fe remaining a body centered cubic crystal structure and thus inferring that the cleavage plane of this group is the (001) crystal plane primarily. Point E represents the point analysis of the grain boundary where the Al element content get near the matching composition. Point G means a composition analysis of the cleavage step, illustrating that Al element exsolution is occurred at the cleavage step as a major reason for alloy cleavage fracture. The points H, I and J are white dots at the fracture surface of the $(Fe_{73}Ga_{24}Al_3)_{99.8}Tb_{0.2}$ alloy for point analysis. The results show that the Tb element content at points H and I are greater than that in the matrix phase remarkably and the Al element content at J point is more than that in the matrix phase, which hint that the fracture of the alloy is cause by the segregation of Al and Tb elements.

The points K and L correspond to white dots at the grain boundary and in the entire grain respectively and point M is a point analysis of the grain boundary. The outcomes show that their relative content of Al element topping than that in the matrix phase, indicating that the fracture reason of the $(Fe_{73}Ga_{23}Al_4)_{99.8}Tb_{0.2}$ alloy accounts for segregation of Al element at different positions. The points N and P symbolize white dots within the grain of $(Fe_{73}Ga_{22}Al_5)_{99.8}Tb_{0.2}$ alloy and the O point is used for point analysis of grain boundaries. The consequences demonstrate that the Tb element content at the N and P points are higher than that in the matrix and the Al element content at the point O exceeds than that in the matrix, which implying that the fracture of the $(Fe_{73}Ga_{22}Al_5)_{99.8}Tb_{0.2}$ alloy is resulted from segregation at the Al element grain boundaries and segregation of Tb elements at grain boundaries or within grains.

In conclusion, the addition of Tb element enhances the tendency of cracking in the alloys. The reasons for the fracture of $(Fe_{73}Ga_{27-x}Al_x)_{99.8}Tb_{0.2}$ alloys include single element segregation of Al element and Tb element, segregation of multiple elements at different positions and Al element exsolution.

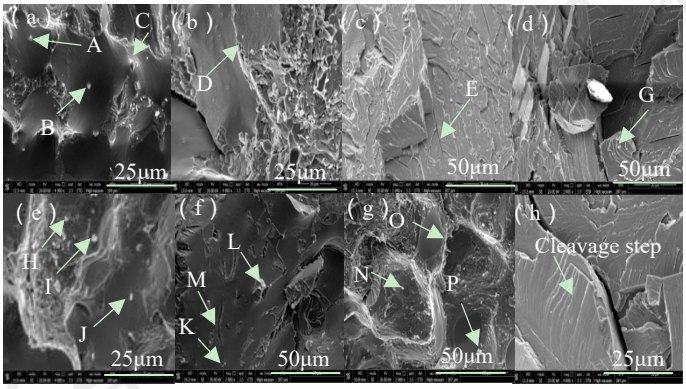

Fig. 8 Fracture morphologies of $(Fe_{73}Ga_{27-x}Al_x)_{99.8}Tb_{0.2}$ alloys at different multiples ((a) x=0, (b) x=1, (c), (d) and (h) x=2, (e) x=3, (f) x=4, (g) x=5; (a), (b), (e) and (h) are 4000 times; (c), (d), (f) and (g) are 2000 times.))

Table 3 EDS analysis of fracture of $(Fe_{73}Ga_{27-x}Al_x)_{99.8}Tb_{0.2}$ al-

loys at different multiples

含量(at%)	Fe	Ga	Al	Tb	含量(at%)	Fe	Ga	Al	Tb
A	63.45	26.54	0	10.01	J	33.76	7.80	58.85	0
B	65.93	23.72	0	10.36	K	57.22	20.58	22.20	0
C	64.25	33.21	0	2.51	L	62.74	21.61	15.65	0
D	65.71	31.18	3.11	0	M	55.70	25.33	18.96	0
E	79.08	19.06	1.92	0	N	47.60	38.86	7.11	6.42
G	0	0	100	0	O	68.87	23.92	7.21	0
H	50.85	40.58	2.27	6.29	P	49.14	38.53	5.96	6.37
I	47.31	41.71	4.08	6.90					

2.8 Vickers Hardness Result

Fig. 9 that presents a trend of first decreasing and then increasing is the Vickers hardness value of the alloys morphing with Al content. The hardness value of the alloys descends when x=0-3 at%, combining with the metallographic preceding photos, the number of irregular cellular crystals is reduced and gradually transmuted to columnar dendrites. In terms of the relevant literature[31], on account of the presence of dendritic crystals, the liquid flow during the final shrinkage process of the alloys in the solidification stage cannot be replenished timely, resulting in the formation of defects such as shrinkage porosity and shrinkage cavity, thus degrading in the mechanical properties of the alloys. Thereby, educing that the hardness value of the alloys decreases in this stage, which may be influenced by columnar dendritic crystals. The maximum value of 339.98 HV is obtained at x=4 at%, based on the metallographic photos of the alloys to infer that the hardness of the alloys is risen since numbers of small hexagonal cellular crystal structure evolved. Furthermore, in comparison to the $(Fe_{73}Ga_{27})_{99.8}Tb_{0.2}$ alloy, except for the alloy of x=4 at%, the hardness value of the $(Fe_{73}Ga_{27-x}Al_x)_{99.8}Tb_{0.2}$ alloys are decreased wholly. According to the scanning electron microscopy results in the anterior text, it is pertinent to the enrichment of Tb elements at grain boundaries, which leads to the diminution of the mechanical properties in the alloys commonly.

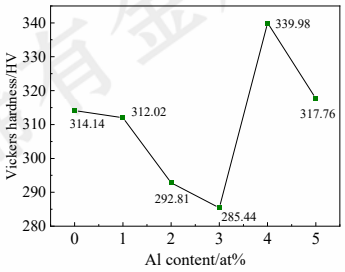

Fig. 9 The curve of Vickers hardness of $(Fe_{73}Ga_{27-x}Al_x)_{99.8}Tb_{0.2}$ alloys varying with Al content

3 Conclusion

(1) The addition of Al element doesn't change the phase structure of $(Fe_{73}Ga_{27})_{99.8}Tb_{0.2}$ alloy and $(Fe_{73}Ga_{27-x}Al_x)_{99.8}Tb_{0.2}$ alloy is still composed of A2 phase and Tb_2Fe_{17} phase. The grain shape of the alloys that preeminently affects the hardness of $(Fe_{73}Ga_{27-x}Al_x)_{99.8}Tb_{0.2}$ alloys is mainly composed of cellular crystal and columnar dendrite.

(2) Comparing with $(Fe_{73}Ga_{27})_{99.8}Tb_{0.2}$ alloy, the $\lambda_{//}$ of alloys at x=1 and x=3 at% increase by 46.5% and 18.3% separately, which is chiefly related to the decrease of lattice constant, the enhancement of (100) orientation and the formation of Tb_2Fe_{17} phase. $(Fe_{73}Ga_{26}Al_1)_{99.8}Tb_{0.2}$ alloy has the characteristics of high *M*s and low *M*r And *H*c in this series of alloys, which can save resources in actual production and reduce production costs.

(3) At room temperature, the tensile strength of $(Fe_{73}Ga_{27})_{99.8}Tb_{0.2}$ alloy can reach 322.8 MPa while the tensile strength of the alloys decreases after adding Al element, but in comparison to the $(Fe_{73}Ga_{27})_{99.8}Tb_{0.2}$ alloy, the elongation of $(Fe_{73}Ga_{26}Al_1)_{99.8}Tb_{0.2}$ alloy increased to 53.4%. The reason of fracture for $(Fe_{73}Ga_{27-x}Al_x)_{99.8}Tb_{0.2}$ alloys include intergranular brittle fracture and cleavage fracture, which results from the segregation of Ga, Tb and Fe. At x=4 at%, the Vickers hardness of the alloys culminates 339.98 HV, surpassing 8.2% than that of $(Fe_{73}Ga_{27})_{99.8}Tb_{0.2}$ alloy.

References

[1] Liu H F, Lim C W, Gao S *et al.* *Mechatronics*[J], 2019, 57: 20

[2] Qiao R H, Gou J M, Yang T Z *et al.* *Journal of Materials Science & Technology*[J], 2021, 84(25): 173

[3] Wang N J, Liu Y, Zhang H W *et al.* *China Foundry*[J], 2016, 13(2): 75

[4] Zhou Z G, Li J H, Bao X Q *et al.* *Journal of Alloys and Compounds*[J], 2020, 826(15)

[5] Clark A E, Restorff J B, Wun-Fogle M *et al.* *IEEE Transactions on Magnetics*[J], 2000, 36(51): 3238

[6] Kellogg R A, Flatau A B, Clark A E *et al.* *Journal of Applied Physics*[J], 2002, 91(10): 7821

[7] Hao H, Wei Z, Gong P et al. *Rare Metal Materials and Engineering*[J], 2022, 51(11): 4265

[8] Mungsantisuk P, Corson R P, Guruswamy S *Journal of Applied Physics*[J], 2005, 98(12): 1

[9] Srisukhumbowornchai N, Guruswamy S *Journal of Applied Physics*[J], 2001, 90(11): 5680
[10] Zhou Y, Wang B W, Li S Y *et al. International Journal of Materials Research*[J], 2008, 99(3): 251
[11] Zhou Y, Wang X L, Wang B W *et al. Journal of Applied Physics*[J], 2012, 111(7)
[12] Li M M, Li J H, Bao X Q *et al. Applied Physics Letters*[J], 2017, 110(14)
[13] Li X L, Bao X Q, Liu Y Y *et al. Applied Physics Letters*[J], 2017, 111(16): 162402
[14] Liu Y Y, Li J H, Gao X X *Journal of Magnetism and Magnetic Materials*[J], 2017, 423(1): 245
[15] Nolting A E, Summers E *Journal of Materials Science*[J], 2015, 50(15): 5136
[16] Emdadi A, Palacheva V V, Cheverikin V V *et al. Journal of Alloys and Compounds*[J], 2018, 758(25): 214
[17] Jiang L P, Zhang G R, Hao H B *et al. Cailiao Rechuli Xuebao/Transactions of Materials and Heat Treatment*[J], 2012, 33(5): 44
[18] He Y K, Ke X Q, Jiang C B *et al. Advanced Functional Materials*[J], 2018, 28(20): 20
[19] Wang R, Tian X, Yao Z *et al. Chinese Rare Earths*[J], 2020, 41(2): 24
[20] Zhang G R, Jiang L P, Hao H B *et al. Chinese Rare Earths*[J], 2013, 34(3): 32
[21] Meng C Z, Wang H, Wu Y Y *et al. Scientific Reports*[J], 2016, 6
[22] Meng C H, Wu Y Y, Jiang C B *Materials & Design*[J], 2017, 130(15): 183
[23] Wu Y Y, Fang L, Meng C Z *et al. Materials Research Letters*[J], 2018, 6(6): 327
[24] Meng C, Jiang C *Scripta Materialia*[J], 2016, 114(15): 9
[25] Li J H, Gao X X, Zhu J *et al. Xiyou Jinshu/Chinese Journal of Rare Metals*[J], 2017, 41(2)
[26] Dai B Y, Wang W W, *Liquid Metal Forming Theory*, Edited, National Dfense Idustry Press, Beijing, 2010: 53: 155
[27] Basumatary H, Palit M, Arout Chelvane J *et al. Scripta Materialia*[J], 2008, 59(8): 878
[28] Zhang J J, Ma T Y, Yan M *Physica B: Condensed Matter*[J], 2009, 404(21): 4155
[29] Clark A E, Wun-Fogle M, Restorff J B *et al. IEEE Transactions on Magnetics*[J], 2001, 37(41): 2678
[30] Yan M, Peng X L, *Fundamentals of Magnetism and Magnetic Materials*, Edited, Zhejiang University Press, Zhejiang, 2006
[31] Yu Y N, *Principle of Metal*, Edited, Metallurgical Industry Press, Beijing, 2003

Al 元素添加对$(Fe_{73}Ga_{27})_{99.8}Tb_{0.2}$合金的微观结构、磁性能及力学性能的影响

杜金超[1,2]，李晓飞[1]，焦佩英[1]，张志广[1]，龚沛[1,*]
(1. 内蒙古工业大学材料科学与工程学院，呼和浩特 010051)
(2. 钢铁研究总院功能材料研究所，北京 100081)

摘　要：已有相关实验表明少量 Al 元素添加能提高合金的伸长率且不会明显降低 Fe-Ga 合金的磁致伸缩应变。此外，由于 Al 价格低于 Ga，采用 Al 替代部分$(Fe_{73}Ga_{27})_{99.8}Tb_{0.2}$合金中的 Ga，还可以降低生产成本。通过真空电弧炉制备$(Fe_{73}Ga_{27-x}Al_x)_{99.8}Tb_{0.2}$(x=0,1,2,3,4,5)合金，研究 Al 添加对合金的微观结构、磁性能和力学性能的影响。结果显示，合金的相结构仍为 A2 相和 Tb_2Fe_{17} 相，其金相组织由胞状晶和柱状树枝晶组织组成。合金的晶格常数降低、(100)取向性增强以及晶界处的 Tb_2Fe_{17} 相对磁致伸缩性能有显著影响。合金的断口形貌为沿晶脆性断裂和解理断裂，产生断裂的原因包括 Tb 和 Al 元素偏析。 $(Fe_{73}Ga_{24}Al_3)_{99.8}Tb_{0.2}$ 合金的平行磁致伸缩应变（$\lambda_{//}$）最高达到 104 ppm。值得注意的是相比$(Fe_{73}Ga_{27})_{99.8}Tb_{0.2}$ 合金，$(Fe_{73}Ga_{25}Al_1)_{99.8}Tb_{0.2}$ 合金的 $\lambda_{//}$提高了 18.3%，伸长率提高了 53.4%，并且$(Fe_{73}Ga_{26}Al_1)_{99.8}Tb_{0.2}$ 合金兼具高饱和磁化强度(*M*s)、低剩余磁化强度(*M*r)和矫顽力(*H*c)等特性，在实际生产中可以降低生产成本；但该合金的抗拉强度和维氏硬度有所下降。因此，研究 Al 元素添加对 Fe-Ga 合金的微观机理对开发 Fe-Ga 合金器件仍具有重要意义。

关键词：$(Fe_{73}Ga_{27})_{99.8}Tb_{0.2}$合金；Al掺杂；微观结构；磁性能；力学性能

作者简介：龚沛，男，1965 年生，博士，教授，内蒙古工业大学材料科学与工程学院 呼和浩特 010051，电话：18048342865，E-mail: 20201100236@imut.edu.cn